DOI: 10.26599/FSHW.2025.9250846

Contents lists available at SciOpen

Food Science and Human Wellness

journal homepage: https://www.sciopen.com/journal/2097-0765

China Food Publishing Co.

Multi-Omics Analysis of Repair Mechanisms in Ohmic Heating–Induced Sublethally Injured *Staphylococcus aureus*: Integrating Lipidomics, Transcriptomics, and Proteomics with Applications in Milk and Vegetable Juice

Han Wang[a], Yingying Sun[a], Yana Liu[b], Yi Li[a], Yi Liu[a], Xingmin Li[a], Ruitong Dai[a,*]

[a] *College of Food Science and Nutritional Engineering, China Agricultural University, Beijing 100094, China*

[b] *College of Food Science and Pharmacy, Xinjiang Agricultural University, Urumqi, Xinjiang 830052, China*

ABSTRACT: Ohmic heating (OH) is a novel rapid heating technology that effectively control *Staphylococcus aureus* (*S. aureus*) survival. However, OH-induced sublethal injury to *S. aureus* pose risks to food safety and public health. Numerous studies have highlighted the importance of membrane repair for bacterial survival. Lipids are the main membranes components, however, their metabolic mechanisms after injured and repair are still unclear. In this study, we compared the lipid compositions of *S. aureus* in untreated, OH-injured, and end-repair states by non-targeted lipidomics and measured malondialdehyde (MDA) content changes, a lipid injury marker. Then, transcriptomic and parallel reaction monitoring analysis were conducted to examine the expression of lipid metabolism-related genes and key enzymes, respectively. The results revealed that OH treatment caused 53 differentially abundant lipids (DALs) increase, including CL, PG, PE, and Cer, while 83 DALs decreased. In the end-repair stage (repair for 5 h), 71 DALs decreased, while only 21 DALs increased. This phenomenon was also reflected in MDA concentration alternations, suggesting that OH-induced lipid homeostasis disruption and oxidative damage were alleviated upon repair. The overall changes trends of lipid biosynthesis enzyme were consistent with lipidomics. Notably, the general changes of lipids metabolism-related genes exhibited an opposite trend: decreased by OH treatment while partially restored after repair. These findings enhanced our understanding of lipid homeostasis in injured bacteria, provided theoretical support for inhibiting injured *S. aureus* repair in food, and promoting OH application in the food industry.

Keywords: Recovery, Sublethally injury, Ohmic heating, Lipid metabolism, Transcriptomics, Parallel Reaction Monitoring

1. Introduction

Staphylococcus aureus (*S. aureus*), one of the most common foodborne pathogens, is a Gram-positive bacterium with a single membrane layer [1]. *S. aureus* can cause foodborne illnesses through forming biofilms and producing various toxins (*e.g.,* enterotoxins and exfoliative toxins) and enzymes (*e.g.,* coagulase), posing an obvious threat to public health and safety [2], and results in considerable economic losses for the food industry. Approximately 420,000 people die annually from foodborne contamination around the world, with 25% attributed to *S. aureus* [3]. Between 2003 and 2017, there were 10,174 reported

***Corresponding author**
dairuitong@hotmail.com

Received 17 June 2025
Received in revised from 24 July 2025
Accepted 4 August 2025

S. aureus-related foodborne disease outbreaks in China, occupied 10.2% of all bacterial infection issues [4]. Therefore, controlling the survival rate of *S. aureus* is urgent to both food industry development and consumer health protection.

In recent years, the growing consumer demand for fresh, healthy, minimally processed foods with preserved flavor has driven the development of novel food processing technologies. One such method, ohmic heating (OH), is a rapid heating technique that converts electrical energy into heat by exploiting the electrical conductivity of food [5]. This allows the food to act as a conductor, thus OH is also referred to as Joule heating. Compared to traditional heating methods, OH not only offers higher energy efficiency and shorter heating times, but also ensures more uniform heating, hence preventing local over-heating and food quality degradation [6]. Owing to its rapid heating, OH declines the effect on food flavor and texture. Additionally, OH has also been proven to effectively control the activity of foodborne pathogens, such as *Escherichia coli*, *Bacillus cereus*, and *S. aureus* [7-9]. However, sublethally injured *S. aureus* cells, which characterized by damaged cell membranes and cell walls, accompanied by leakage of intracellular substances and weakened stress resistance [10]. Under favorable conditions, the injured cells can initiate repair processes to restore their virulence and resistance to adverse environmental factors [11] Therefore, understanding the repair mechanisms of injured *S. aureus* is crucial for mitigating food safety risks, reducing economic losses in the industry, and protecting consumer health. Previous studies on bacterial repair mechanisms have mainly focused on inducing sublethal injury and evaluating the effect of repair conditions (*e.g.,* temperature, pH, and nutrients). However, molecular-level investigating remains limited and often involve short repair intervals. For example, Shao et al. (2022) reported that OH-induced sublethally injured *S. aureus* cells could be completely repaired in nutrient broth (NB) within 3 h at 25℃ or 37℃, with minimal recovery observed at 4℃; repair was faster at pH 7 compared to pH 6 and 8 [11]. Similarly, sublethally injured *E. coli* f induced by high hydrostatic pressure were fully repaired within 2 h in tryptone soya broth or buffered peptone water, whereas recovery in PBS took over 5 h [12].

The cell membrane plays a critical role in bacterial defense against external stress and survival, and the membrane damage is a hallmark of sublethally injury and is responsible for their inability to grow on selective-media [13]. As an essential component of the cell membrane, lipids are involved in energy conversion and metabolism, membrane fluidity regulation, and signal transduction. However, changes in lipid composition and content in *S. aureus* following OH-induced injury and repair, as well as the underlying mechanisms, remain unclear.

In the field of food microbiology, the widespread application of omics technologies has significantly contributed to revealing the molecular mechanisms behind bacterial responses to different environmental conditions. These techniques not only minimize the biases inherent in traditional culturing methods but also provide a more comprehensive characterization of microbial communities and their products [14]. Among these techniques, non-targeted lipidomics allow for the analysis of lipid composition and quantity in specific time and space, while high-throughput transcriptomics comprehensively reflects gene expression changes.

To date, no studies have explored the metabolic changes in lipids in *S. aureus* after injury and repair using multi-omics approaches. Therefore, this study aims to focus on the molecular mechanisms behind the changes in *S. aureus* lipid profile before and after repair through the combined analysis of lipidomics analysis, transcriptomics, and parallel reaction monitoring (PRM).

2. Materials and Methods

2.1 Bacterial strain and cultural conditions

2.1 Microbial preparation

In this experiment, *S. aureus* ATCC 6538 was purchased from the Shang Hai Huiyun Biological Co., Ltd. The activated *S. aureus* was cultured in NB (Beijing Solarbio Co., Ltd) in a shaker (12 h, 37℃), then 2 mL bacterial solution was transferred to 200 mL new NB medium, and continue incubated at 37℃ until reaching mid-exponential growth (3.5 h). Subsequently, the *S. aureus* cells were centrifuged (8000 × *g*, 4℃, for 10 min), washed twice with phosphate buffered saline (PBS), re-suspended and kept in a 4℃ refrigerator for further experiments. The eventual concentration of *S. aureus* cells was about 10^8 CFU/mL.

2.2 Ohmic heating treatment and repair process

The OH process parameters and restoration condition were aligned with the published work of our laboratory [9]. Simply, 160 mL PBS bacterial suspension was transferred into the heating unit, with the voltage gradient and frequency preset to 10 V/cm and 50 Hz, respectively. After OH had been running for approximately 100 s, the final temperature reached 55.5℃. Meanwhile, the largest proportion of sublethally impaired bacteria were obtained (Equation 1)[9], then the *S. aureus* cells suspension was quickly cooled to 4℃. Subsequently, the repair experiments were undertaken. In particular, the injured *S. aureus* cells were resuspended in an equal volume of NB and incubated at 37℃ in a temperature-controlled shaker until reaching the stable phase, referred to as “the end repair stage” in this experiment. The cells were then washed twice with PBS, and the precipitate was collected by centrifugation (8000× *g*, 4℃, 10 min). Subsequently, the precipitate was transferred to a sterile cryogenic storage tube, rapidly cooled in liquid nitrogen, and stored at -80℃ for further analysis.

$$The\ \ injury\ \ ratio\ \ (\%) = 100\ -\ \frac{CFU\mid mL_{NA-NaCl}}{CFU\mid mL_{NA}} \times 100 \qquad (1)$$

Where CFU/mL $_{\text{NA-NaCl}}$ was the colony forming unit on the NA supplemented with 10% NaCl; CFU/mL $_{\text{NA}}$ was the colony forming unit on the NA.

2.3 Raman spectra analysis

Freeze-dried *S. aureus* samples in different states were placed on a sample stage. A laser beam is emitted through laser source to illuminate the sample. The laser light is scattered after interaction with the sample, where the inelastic scattered light is collected by detector. The collected Raman scattered light signals were processed by HORIBA Scientific LabRAM HR Evolution to obtain Raman spectra.

2.4 Lipidomics analysis

2.4.1 Sample preparation

Firstly, different states of *S. aureus* cells sample were weighed precisely 50 mg, mixed with 280 μL of methanol: water solution (*v/v* = 2: 5) and 400 μL MTBE. Before extraction, a 6 mm grinding bead was added to every sample, followed by processing with a high-throughput tissue grinder (Wonbio-96c, Shanghai wonbio Technology Co., Ltd.) (-10℃, 50 Hz, 6 min) and sonication process (4℃, 40 kHz, 30 min). The samples were placed at -20℃ for 30 min and centrifuged at 13,000 × *g* at 4℃ for 15 min. The lipid extract contained in the upper phase was transferred to a new tube and blown dry with nitrogen. The samples were sonicated in a 5℃ water bath with 100 μL of isopropanol: acetonitrile (1: 1 = *v/v*) sample solution. The collected lipids were centrifuged and the supernatant was pipetted into a sample container. Ultimately, 2 μL per sample was pumped into the UHPLC-MS/MS system for further analysis.

2.4.2 UHPLC-MS/MS analysis

The samples were characterized by LC-MS using a Thermo UHPLC-Q Exactive HF-X system and an Accucore C30 column (100 mm × 2.1 mm *i.d.*, 2.6 μm; Thermo) at Majorbio bio-pharma Technology Co., Ltd (Shang, China). Mobile phase A was 50% acetonitrile in water (0.1% formic acid and 10 mmol/L ammonium acetate), and mobile phase B was acetonitrile/isopropanol/water (0.02% formic acid and 2 mmol/L ammonium acetate). The injection parameters of the standard are: volume: 5 μL, column temperature: 40℃; the flow rate is always 0.4 mL/min. The total chromatographic separation time is 20 min, all samples were kept at 4℃ during analysis. The ratio of A to B over time is shown in Table S1. The MS data were gained through a Thermo UHPLC-Q-Exactive HF-X desktop orbitrap MS outfitted with a heated electrospray ionization source in positive and negative ion modes. The specific preferred conditions are shown in Table S2.

2.4.3 Data processing and lipid identification

Raw data was inserted into LipidSearch (Thermo Fisher, USA) for s series steps, including basic filtering, peak recognition, integration, time adjustment, peak matching, *etc.,* to obtain retention time, mass-to-charge ratio, and peak intensity. MS and MS/MS information was matched with a lipid database, and the MS tolerance and fragment error ranges were both < 10 ppm. The m-score threshold was 2.0, and four distinct grades were applied for ID quality filtration. The data matrix generated by the preprocessing results includes lipids, retention times (RT), mass-to-charge ratio (m/z) values, and peak intensities. To reduce the errors caused by sample preparation and instrument instability, a normalization method was applied to standardize the response intensity of the sample MS peaks, and a normalized data matrix was obtained for subsequent analysis. Lastly, a variance calculation was performed on the matrix file, including principal component analysis (PCA) and orthogonal partial least squares discriminant analysis (OPLS-DA). The selection of differentially accumulated lipids (DALs) was determined based on the variable importance in projection (VIP) acquired from OPLS-DA and *p*-value, with VIP > 1 and $P < 0.05$.

2.5 Determination of oxidation resistance and malondialdehyde (MDA) in S. aureus cells

The intact, injured, and repaired *S. aureus* cells were processed according to the method shown in Part 2.2. The bacteria were mixed with extract solution and then crushed by ultrasonication: ice bath, 300 W, 5 s work, and 10 s pause, a total of 10 min. Afterwards, the supernatant was collected (centrifugation: 12, 000 × *g,* 4℃, 3 min) and placed on ice for further research. The supernatant was mixed with matching test reagents following the manufacturer's instructions (BC0025, Beijing Solarbio Science & Technology Co., Ltd.), and the absorbance was recorded at the wavelengths of 532 nm and 600 nm, which were applied to calculate the concentration of MDA.

2.6 Transcriptomic analysis

Untreated (UT group), injured (SI group), and end repair stage (R_E) *S. aureus* cells obtained from Part 2.1 and 2.2 were utilized for transcriptomics and metabolomics analysis. Ribosomal RNA (rRNA) depletion was carried out by the RiboCop rRNA Depletion Kit for Mixed Bacterial Samples (lexogen, USA), and fragmentation buffer was successively supplemented to cleave all mRNA into short fragments. Afterward, double-stranded cDNA was composited with random hexamer primers (Illumina). dUTP replaced dTTP in the generation of the cDNA second strand. The RNA-seq transcriptome libraries were prepared using the Illumina® Stranded mRNA Prep with Total RNA, Ligation (San Diego, CA) approach. The paired-end RNA-seq database was sequenced with Illumina Novaseq 6000 (Illumina, Inc., San Diego, CA, USA). Initial pictures were manipulated to sequences, baseline calls, and quality value computations. Clean sequences were acquired by eliminating low-quality sequences, reads containing > 10% unidentified bases, and reads overwriting adapter sequences. The data generated by the Illumina platform was used for bioinformatics analysis. All analyses were conducted through an online platform (www.Majorbio.com). The original materials were initially analyzed via in-house scripts. Gene targeting of *S. aureus* ATCC 6538 was mapped using Bowtie2 (http://bowtie-bio.sourceforge.net/bowtie2/index.shtml). Differential expression analysis between two groups (3 biological replicates per group) was undertaken using the DESeq, DESeq2, or edgeR software package. False discovery rate (FDR) was calculated to correct the *p*-values obtained from independent statistical hypothesis tests. Differentially expressed genes (DEGs) were identified as those with FDR < 0.05 and fold change (FC) ≥ 2 or < 0.5. KEGG enrichment analysis was applied to metabolic pathways enriched for DEPs.

2.7 Parallel reaction monitoring (PRM) analysis

Frozen bacterial *S. aureus* samples were placed on ice, protein lysate (8 M urea, 1% SDS, containing protease suppressor) was added, ultrasonicated on ice, lysed, and then the supernatant was obtained by centrifugation (12,000 × *g*, 4℃ for 30 min). Protein quantification was achieved by BCA method and analyzed by SDS-PAGE. 100 μg of protein solution was removed and TEAB was added at a final concentration of 100 mmol/L, then TCEP (final concentration 10 mmol/L), and incubated at 37℃ for 60 min. After joining IAM and pre-tempered acetone, the mixture was centrifuged to obtain the precipitate. Following lysis and enzyme cleavage, the peptides were evaporated to dryness using a vacuum concentrator. The peptides were desalted, then the solvent was dried again by evaporation using a vacuum concentrator.

Peptide quantification was according to the manufacturer's instructions (Thermo Fisher, 23275). Subsequently, peptide segments were analyzed using a FULL MS-PRM MS assay. The data acquisition software was Thermo Xcalibur 4.7 (Thermo, USA), the reverse-phase column information: uPAC High Throughput column (75 μm × 5.5 cm, Thermo, USA), the chromatographic separation time and the flow rate was 24 min and 0.75- 2.5 μL, respectively. The FULL MS scan range (m/z) and the resolution was 350- 200 and 240000, respectively. Afterward, the Skyline software was used to search the database, and for the identified target proteins, the peptides with better mass were selected for quantitative experiments.

2.8 Applications in parsley-kale juice and tomato juice at different temperatures

Bacterial pellets were obtained following the method described in section 2.2. Bacteria were resuspended in equal volumes of milk (Beijing Sanyuan Foods Co., Ltd.), parsley-kale juice and tomato juice (Qingdao Punomis Beverage Co., ltd.). The juices were then divided into two groups and stored at 4℃ and 25℃, respectively. The number of intact bacteria versus sublethally damaged bacteria was recorded at 0, 6, 15, 24, 48 and 72 h.

2.9 Statistical analysis

Data were displayed as mean ± SD. Data analysis was performed using SPSS 26.0 (IBM Corporation, Chicago, IL). Student's t-tests were applied to versus differences between the two groups. P-value < 0.05 was regarded as statistically significant. Visualization of results was made by GraphPad Prism 8.2.1 (GraphPad Software Inc., San Diego, CA).

3. Results

3.1 Raman spectra analysis of untreated, injured, and repaired S. aureus

In this study, after OH treatment, there were 5.84 and 3.48 Log CFU/mL *S. aureus* were detected on NA and NA-NaCl, respectively, with an injury ratio > 95%. Raman spectra analysis was performed to obtain insight into changes in cell surface chemical bonding and composition of injured and repaired *S. aureus* cells. As depicted in Figure 1, the signals primarily correspond to the cell membrane and internal structure, including proteins (876, 889, 1000, 1279, and 1685 cm^{-1}), lipids (1162, 1520, 1514, 2920 cm^{-1}), polysaccharide (1184 cm^{-1}), peptidoglycan (534 cm^{-1}), and nucleic acid (727 and 876 cm^{-1}). The observed changes suggest that OH treatment disrupts membrane fatty acid homeostasis and causes damage to protein structures and carbohydrate backbones. This indicated that the cell membranes and cell walls of *S. aureus* were compromised, leading the bacteria into a sublethal state. In addition, fluctuations in signal absorption during the repair process potentially reflect the restoration of cell structure compared to unrepaired *S. aureus* cells. These findings are consistent with previous research, which showed that the damaged cellular structure of OH-treated *S. aureus* can recover during the repair phase [10].

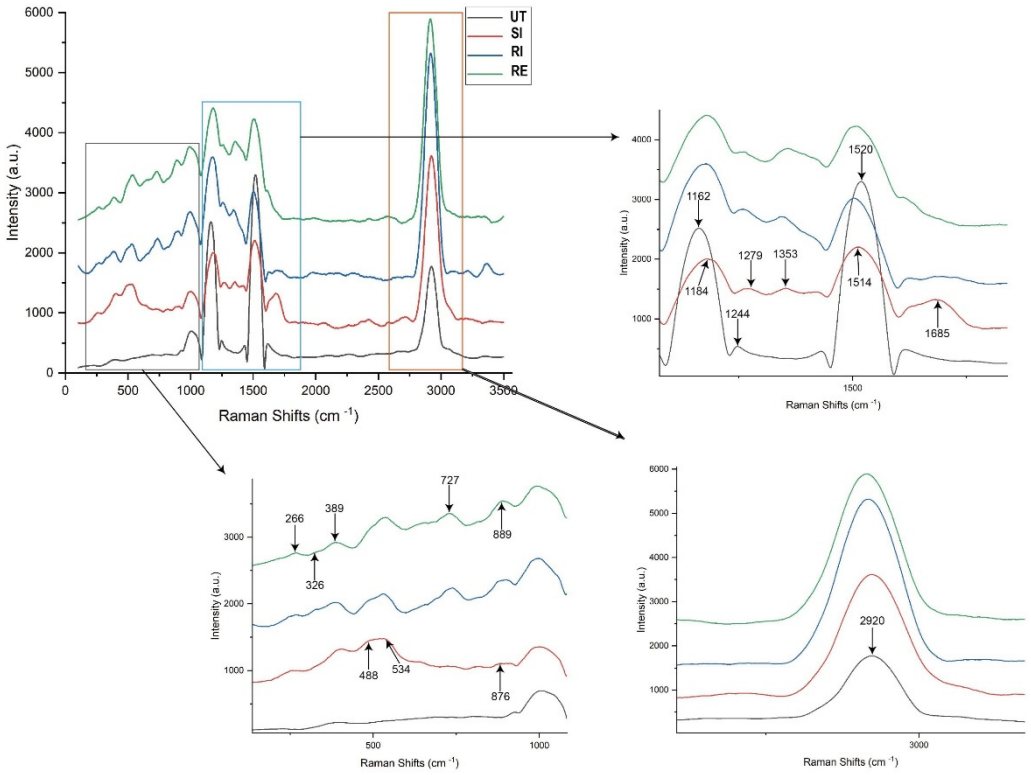

Figure 1. Raman spectra of *S. aureus* in different states. UT: untreated *S. aureus*; SI: OH-induced sublethally injured *S. aureus*; RI: injured *S. aureus* in early repair stage; RE: repaired *S. aureus*.

3.2 Comprehensive lipidomics analysis of untreated, injured, and repaired S. aureus

After bacterial lipids were obtained, the lipid profile alternations of *S. aureus* in different states were analyzed by UHPLC-MS/MS (Figure 2). As illustrated in the PCA score plot in positive (Figure 2B) and negative modes (Figure S1), after OH treatment, the sample ellipses of injured *S. aureus* are strikingly separated from those of untreated healthy cells, suggesting that OH-marked changed *S. aureus* lipid composition. Instead of separating from each other, the sample ellipses of R_E group partially overlap with the sample ellipses of SI group. This phenomenon uncovers that the lipids of *S. aureus* cells changed after repair in NB, while there are still differences from the intact *S. aureus* cells. In addition, the results of OPLS-DA model showed that samples of the UT and R0 groups were obviously separated in both positive and negative ion modes, suggesting that the sublethal injury caused by OH process has disrupted the lipids profile of *S. aureus* (Figure S2 C and D). Similarly, separation was also found between the injured and repaired *S. aureus* cells, indicating that lipids profile disturbances might be alleviated (Figure S2 A and B). Permutation tests were used to examine the fitness and reliability of the OPLS-DA model's predictability and reliability (Figure S3), which is reflected in the values of R2 and Q2. Besides, the negative intercept of the Q2 regression line was less than 0 in both positive and negative modes, showing that overfitting does not exist in the OPLS-DA model (Figure S3 A-D). After the data had been validated and integrated, DALs were confirmed under the criteria: $P < 0.05$ and VIP > 1. As illustrated in Figures 2C and 2D, compared to untreated *S. aureus* cells, OH process caused 83 significant increases and 53 decreases DALs in injured *S. aureus*. When *S. aureus* was

repaired to the stable-repair phase, there was a dramatic elevation of 21 DALs and 71 DALs decrease compared to injured bacteria that were not repaired. In addition, Figures 2E and 2F illustrate the significance of DALs in the form of bubbles, in which each bubble size represents a differential lipid size. The y-axis, x-axis, and bubble size denoting the lipid subclasses, the difference magnitude, and lipids number, respectively, and the lipid profiles on both sides of the X-axis 0 scale line of the bubble and volcano plots are consistent. Concretely, 23 lipid categories differed in the UT-SI group, while 20 lipids in SI-R_E group. The clustering heatmap shows that intra-group differences were smaller than inter-group differences (Figure 2G and 2H), and the DALs distribution is consistent with the presented findings in volcano and bubble plots. In short, based on the quantitative changes of DALs in different periods, it can be found that OH treatment significantly changed the lipid profile of *S. aureus* and might produce a stress response, leading to an overall upward trend in the DALs, and the remarkable downregulation of lipid molecules in SI-R_E group indicate that *S. aureus* lipid composition changed significantly after repair.

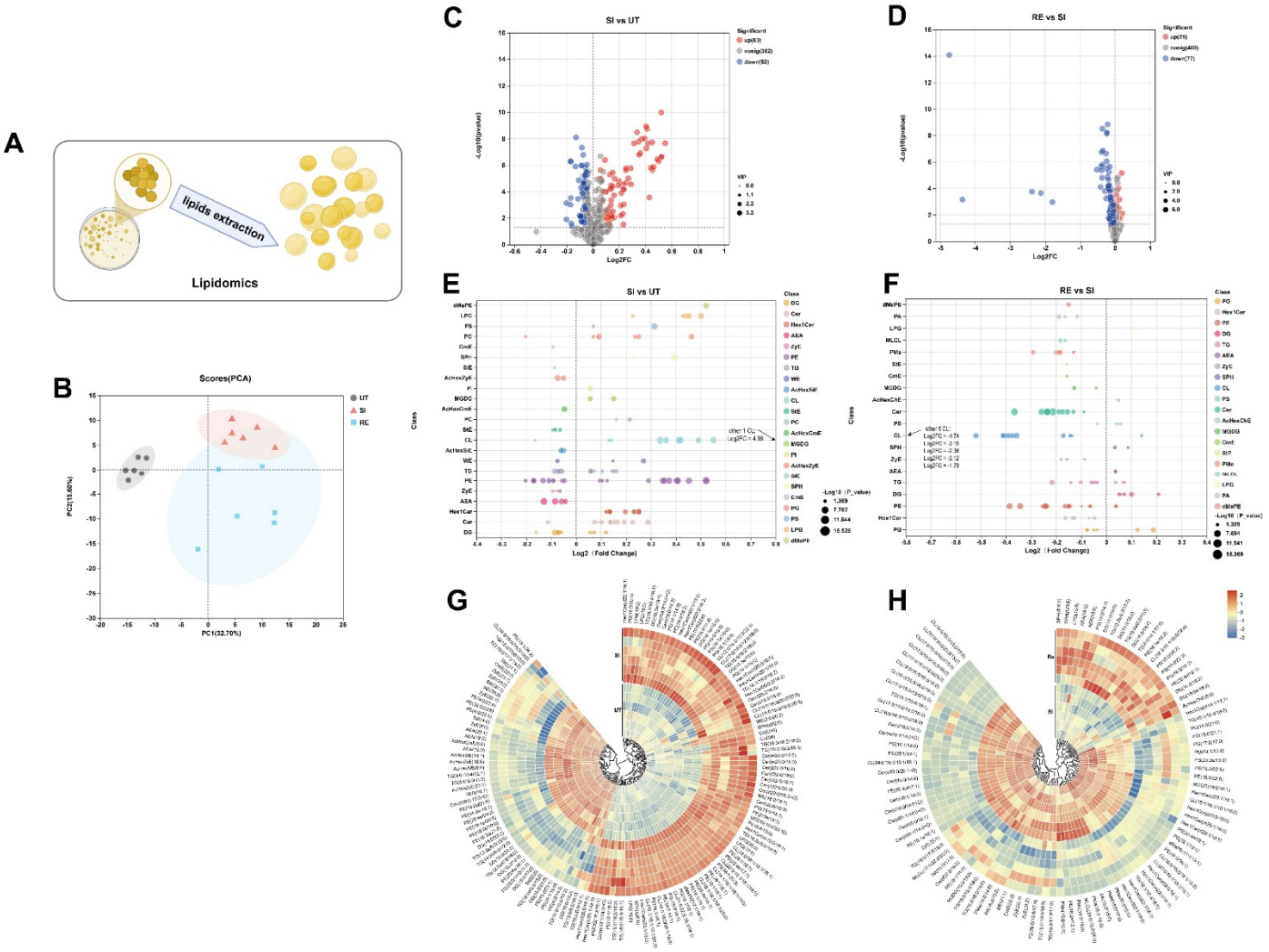

Figure 2. (A) *S. aureus* lipids were extracted for lipidomic analysis; (B) Principal component analysis (PCA) of samples from different groups in positive mode; (C) The volcano plots of DALs of *S. aureus* between SI vs. UT and (D) R_E vs. SI; (E) Bubble chart of DALs of *S. aureus* in SI vs. UT and (F) R_E vs. SI. (G) DALs of *S. aureus* circle clustering heatmap of SI vs. UT and (H) R_E vs. SI. DALs: differentially abundant lipids; UT: untreated *S. aureus*; SI: OH-induced sublethally injured *S. aureus*; R_E: repaired *S. aureus*.

As shown in Figure 3A, a total of 495 lipid molecules were identified, distributed across 5 categories (glycerolipids (GL), glycerophospholipids (GP), sphingolipids (SP), fatty acyls (FA), and sterol lipids (SL)), including 36 subclasses ((triglyceride (TG), diglyceride (DG), mnogalactosyldiacylglycerol (MGDG), digalactosylmonoacylglycerol (DGMG), monoglyceride (MG), and monogalactosylmonoacylglycerol (MGMG); cardiolipin (CL), phosphatidylethanolamine (PE), posphatidylglycerol (PG), phosphatidylinositol (PI), phosphatidylserine (PS), monolysocardiolipin (MLCL), phosphatidylmethanol (PMe), phosphatidylcholine (PC), lyso-PG (LPG), phosphatidic acid (PA), lyso-PC (LPC), and dimethylphosphatidylethanolamine (dMePE); ceramides (Cer), monohexosyl ceramide (Hex1Cer), sphingomyelin (SPH), and gangliosides (GD2, GM1); anandamide (AEA), wax ester (WE), (O-acyl)-hydroxy fatty acid (OAHFA), and coenzyme (Co); stigmasterylester (StE), zymosterol (ZyE), cholesteryl methyl ester (CmE), sitosteryl ester (SiE), acetate-hexanoate cholesteryl ester (AcHexChE), AcHexSiE, AcHexZyE, and AcHexCmE. Among them, the primary lipids that make up the major portion of *S. aureus* are TG, CL, PE, DG, Cer, and PG. The lipids molecule number distribution across different groups is displayed in Figure 3 B-D, and the outcomes illustrate that although the lipids distribution of *S. aureus* changes in various states, the lipids accounted for the greater proportion of all groups were all TG, CL, PE, PG, DG, and Cer. The detailed lipid profile information of each group is shown in Table S3, and Figure 3E exhibits the lipids that were detected in the untreated, injured, and repaired states of *S. aureus* cells. For example, CL, Cer, and PE concentrations were considerably raised post-injury and then declined after repair, while AEA showed the opposite trend. In addition, MDA, associated with lipid oxidation, reflects damage to bacterial cell membranes. In this study, the MDA content significantly increased following OH treatment while decreasing at the end repair phase (Figure 4), which also reflected that OH-induced cell membrane disruption was reversed by repair in NB. Collectively, *S. aureus* lipid profiles and subclass composition altered after OH treatment and repair in NB, and OH-induced oxidative damage to bacterial lipids.

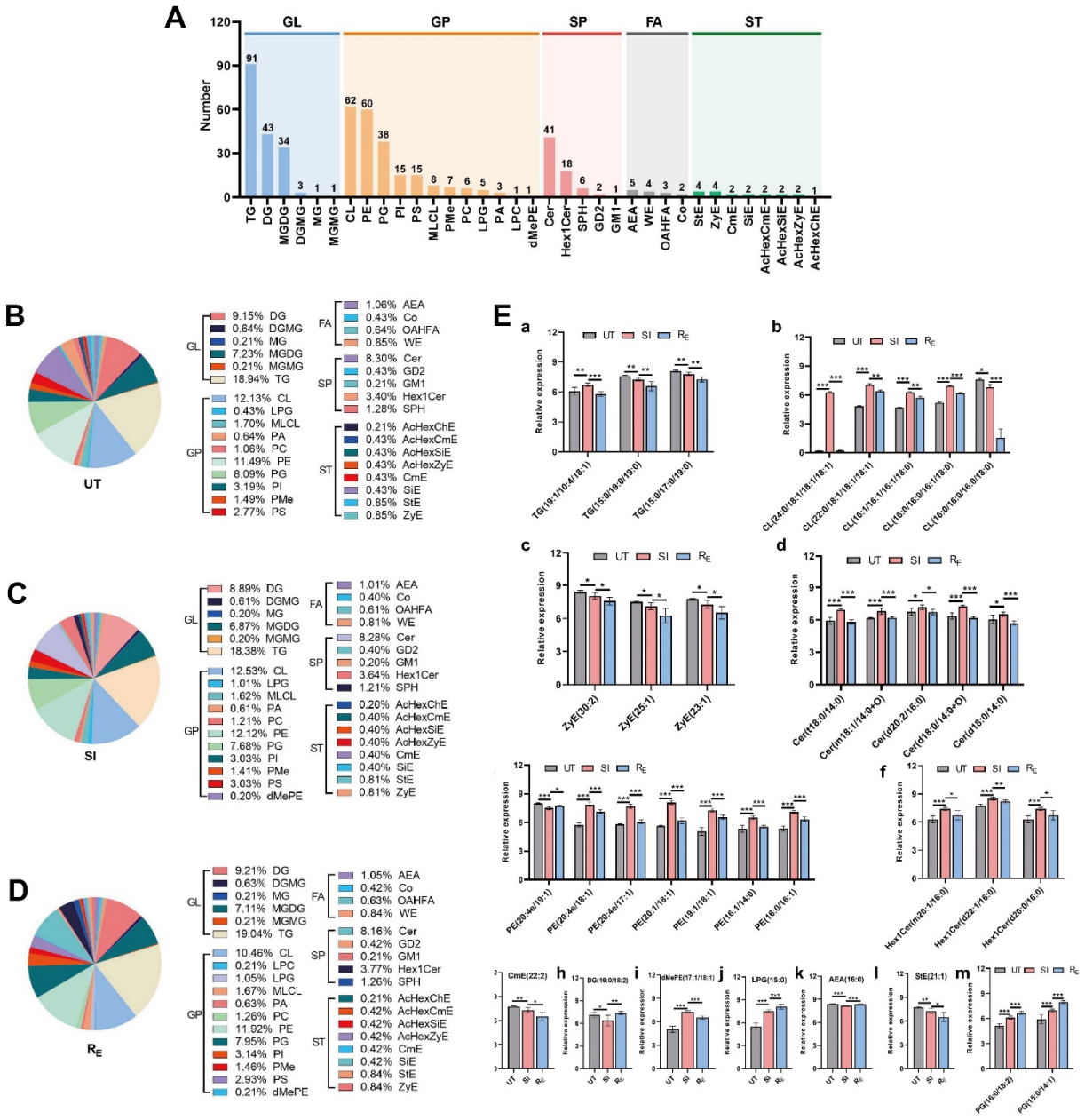

Figure 3. Statistics analysis of lipid classes and species. (A) 495 lipid species classified into 36 lipid classes in *S. aureus*. (B-D) Proportional distribution of lipid classes in each group. (E) Lipids co-existing in untreated, OH-induced sublethally injured, and repaired *S. aureus* cells. UT: untreated *S. aureus*; SI: OH-induced sublethally injured *S. aureus*; R_E: repaired *S. aureus*. Significant correlations are marked by $*P < 0.05$; $**P < 0.01$; $***P < 0.001$.

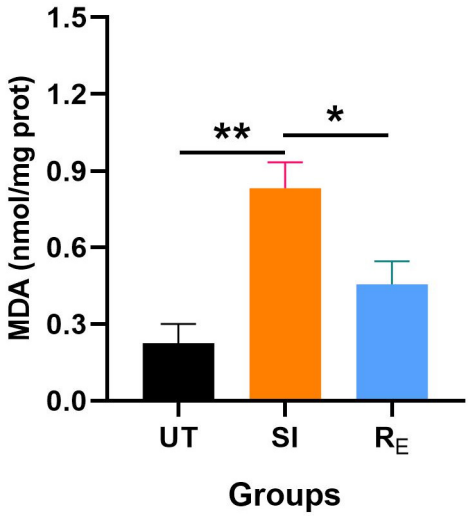

Figure 4. Alternations in intracellular MDA concentration in untreated, OH-induced sublethally injured, and repaired *S. aureus* cells. UT: untreated *S. aureus*; SI: OH-induced sublethally injured *S. aureus*; R_E: repaired *S. aureus*. Capital letters a ~ e represent the significant difference under different recovered time ($P < 0.05$). Significant correlations are marked by *$P < 0.05$; **$P < 0.01$; ***$P < 0.001$.

A complete cell membrane is essential for bacterial survival under stressf. Among the lipids identified in this study, GPs are the main membrane components and play vital roles in membrane fluidity and protein function. Furthermore, GPs also influence the synthesis pathways of phospholipids by modulating phospholipase activity [15]. In the membranes of bacteria, GPs are primarily included CL, PE, and PG, which constitute 12.53% (62/495), 12.12% (60/495), and 7.68% (38/495) of total lipids, respectively. CL is involved in membrane protein localization and electron transport, contributing to energy metabolism [16, 17]. PE supports transmembrane proteins stability and affect heat resistance and oxidative stress tolerance[18, 19], while PG, due to its negative charge, helps maintain membrane strength and temperature resistance [20, 21]. In OH-injured *S. aureus*, CL (11/12 species) and PG (6/7 species) lipids were significantly upregulated, whereas PE exhibited a balanced response (12 up- and downregulated lipids). Additionally, the concurrent increase in MDA levels after OH treatment and its decrease upon repair may be associated with changes in PG and PE content. Unlike previous findings in *Bacillus cereus,* where CL, PE, and PG decreased after OH exposure [22], our results suggest that the upregulation of CL and PG in *S. aureus* may reflect a stress response triggered by moderate membrane damage, leading to enhanced the synthesis of these lipids. PC, another key GP involved in membrane stability and choline metabolism [23], was also regulated (3/3 species) following OH treatment. Among GLs, TG and DG were the most abundant, constituting 18.38% (91/495) and 8.69% (43/495) of the total lipids, respectively. DG regulates TG metabolism. SPs play roles in membrane stability and signal transduction [24–26], represented 8.28% (41/495) of total lipids. Cer (13/14 species) was strongly upregulated after OH exposure, while TG and DG exhibited mixed trends. During the repair phase, most DALs (77/99) were downregulated, including TG (9/12), PG (4/6), and Cer (10/10), whereas all detected DG species (5/5) were significantly upregulated [24-26]. These findings highlight dynamic lipid remodeling in response to OH-induced stress and repair, offering insight into the lipid requirements of *S. aureus* under different physiological states. Specifically, OH treatment induces the up-regulation of lipid synthesis-related enzymes,

leading to increased levels of certain lipids. This may reflect a bacterial stress response, where certain proteins are activated and the key lipids components are up-regulated to help counteract environmental stress. However, once the cells are placed in a suitable environment, this adversity is alleviated. By the end of the repair phase, the process enters a stable phase, as evidenced by decreased activity of lipid synthesis-related enzymes and reduced lipid content.

3.3 Comprehensive analysis of transcriptomic response of S. aureus after OH-induced injury and during repair

Investigating lipid metabolism changes at a single level is insufficient to comprehensively reveal the underlying mechanisms. Thus, using transcriptomics to assess the expression changes of lipid metabolism-related genes might provide a valuable complementary approach. The RNA of *S. aureus* was extracted for transcriptomics analysis (Figure 5A). After OH treatment, a total of 1,355 DEGs were found, including 760 up-regulation and 595 down-regulation (Figure 5B). By contrast, *S. aureus* cells at the end-repair stage exhibited 1470 DEGs (740 upregulated and 730 downregulated) versus the unrepaired one. Cluster analysis revealed that the gene expression differences between groups were greater than differences among samples within groups, and the trend was consistent with volcano plot results (Figure 6A and B). Venn diagrams were applied to show DEG distribution across different groups (Figure 5D). Specifically, 764 DEGs were identified as common to both the injured (UT-SI) and initial repair stages (SI-R_E), and the unique DEGs for the groups UT-SI and SI-R_E were 502 and 561, respectively. To focus on exploring the lipid metabolism changes, 24 relevant DEGs were screened and analyzed by clustering to clarify the change trends of these DEGs (Figure 5A and B). Specifically, 22 lipid metabolism-related genes were downregulated by OH treatment, including *fabG*, *fabH*, *fabD*, *accA*, *accB*, *glpK*, *plsX*, *etc.*, with only *pldB* and *tagD* upregulated. After recovery in NB until the stable-repair stage, the overall trend of gene expression shifted from declining to increasing, as evidenced by 18 significant up-regulations and 6 down-regulations. The results of KEGG pathways analysis indicate that these DEGs were mainly enriched in glycerophospholipid, glycerolipid, fatty acid metabolism pathways, and energy-related metabolism pathways, such as pyruvate metabolism and carbon fixation pathways in prokaryotes (Figure 6C and D).

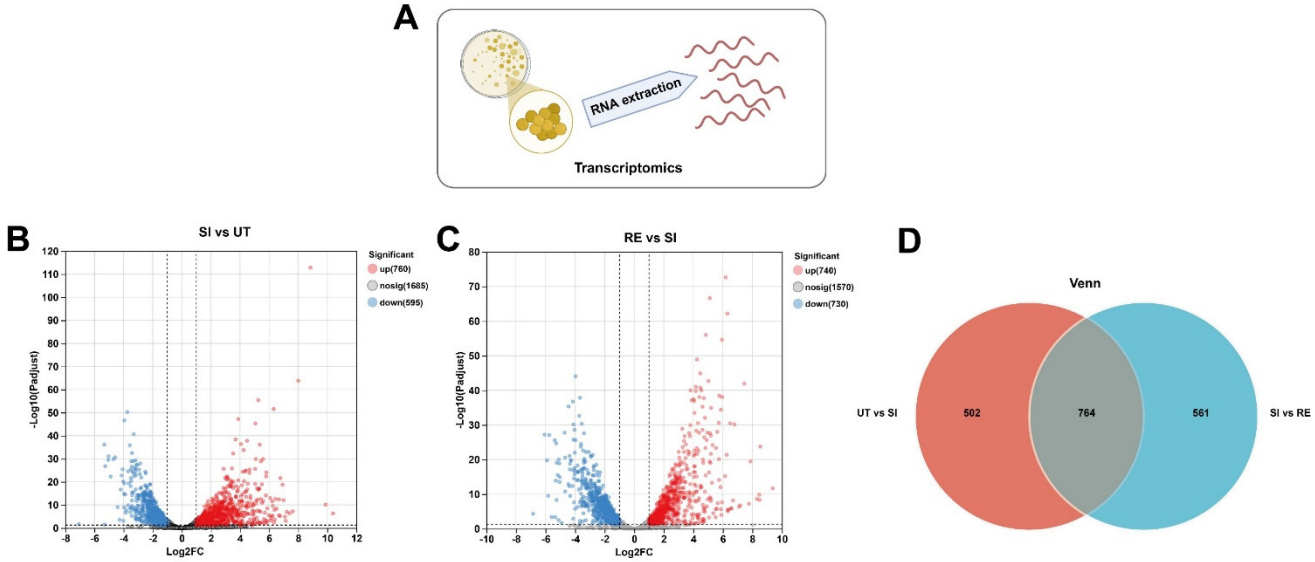

Figure 5. (A) *S. aureus* RNA was extracted for transcriptomics analysis. (B) The volcano plots of DEGs of *S. aureus* between SI vs. UT and (C) R_E vs. SI; (D) Analysis of DEGs with Venn's diagrams. DEGs: Differentially expressed genes; UT: untreated *S. aureus*; SI: OH-induced sublethally injured *S. aureus*; R_E: repaired *S. aureus*.

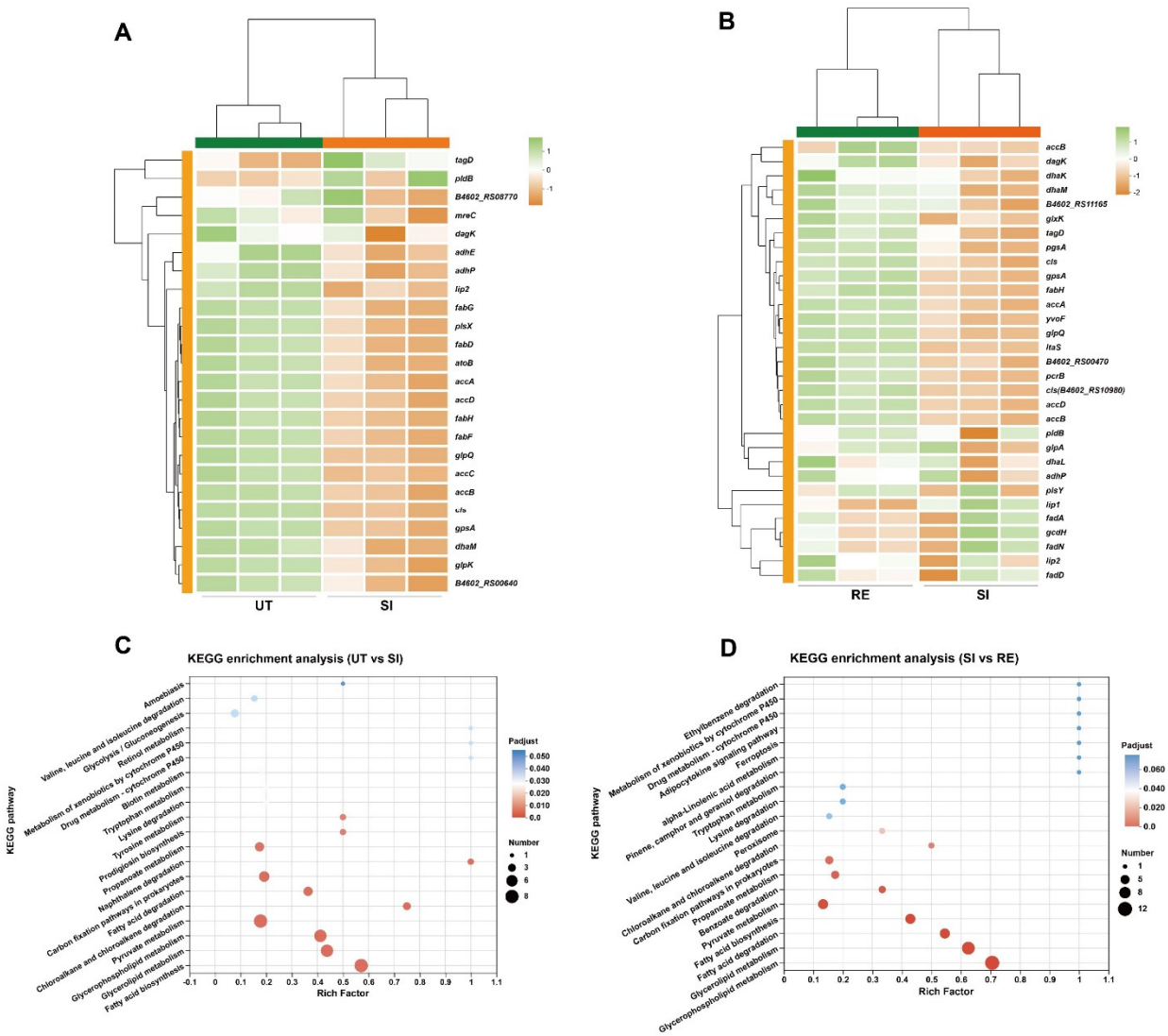

Figure 6. (A) Lipid metabolism-related DEGs of *S. aureus* clustering heatmap of SI vs. UT; and (B) R_E vs. SI; (C) KEGG enrichment analysis of these DEGs between SI vs. UT; and (D) R_E vs. SI. DEGs: differentially expressed genes; UT: untreated *S. aureus*; SI: OH-induced sublethally injured *S. aureus*; R_E: repaired *S. aureus*.

Numerous studies have shown that sublethal injury to bacterial membranes leads to alterations in lipid profiles and disruptions in lipid metabolism [27-29]. In the initiation phase of fatty acid synthesis (Figure 6), the *accABCD* genes encode enzymes that catalyze the conversion of acetyl-CoA to malonyl-CoA. This compound is subsequently converted into malonyl-ACP by FabD (encoded by *fabD*). Both acetyl-CoA and malonyl-ACP serve as substrates for FabH, which converts them into acetoacetyl-ACP—an essential precursor for downstream carbon chain elongation. In the elongation phase, FabG (encoded by *fabG*) functions as a balancing enzyme, while FabI (encoded by *fabI*) acts as a rate-limiting enzyme, catalyzing the reduction of β-ketoacyl-ACP to β-hydroxyacyl-ACP and trans-2-enoyl-ACP to acyl-ACP, respectively [30]. The resulting acyl-ACP is then utilized in the transacylation pathway for phospholipid synthesis, facilitated by PlsX and PlsY (encoded by *plsX* and *plsY*). In the final stage of phospholipid biosynthesis, Cls (*cls*), MprF (*mprF*), and PgsA (*pgsA*) are responsible for the synthesis of CL, LPG, and phosphatidylglycerophosphate (PG-P), respectively.

In the present study, OH treatment significantly downregulated genes involved in lipid metabolism. By the end of the repair phase, most of these genes exhibited overall upregulation, except for *fadD*, *fadN*, and *fadA*, which remained markedly suppressed. These results suggest that OH inhibited key enzymes in *S. aureus* fatty acid and lipid metabolic pathways, and this inhibition was partially alleviated during recovery in nutrient broth.Consistent with previous findings by Pang et al. [27], who reported decreased expression of lipid metabolism–related genes (e.g., *fabI*, *fabH*, *fabF*, *plsX*, *plsY*, *cls*, *mprF*) and corresponding enzymes and lipid levels after membrane damage, it is generally expected that gene expression, enzyme activity, and lipid content would decrease upon injury and increase during repair. However, in this study, we observed an inverse relationship: while gene expression decreased after OH treatment and increased during repair, lipid followed the opposite pattern. This discrepancy suggests the involvement of complex post-transcriptional or post-translational regulatory mechanisms. Further studies are needed to directly examine the proteins translated from these genes and clarify their roles in modulating lipid metabolism under sublethal stress.

3.4 PRM analysis of S. aureus after OH-induced injury and during repair

As can be seen in Figure 7, to further investigate the lipid change mechanism in different periods of *S. aureus*, the expression levels of 14 pivotal enzymes on the fatty acid and lipid metabolism pathways (Figure 8) were targeted detection by PRM. For fatty acid synthesis initiation pathways, the expression levels of acetyl-CoA carboxylase biotin carboxylase (AccC), acetyl-CoA carboxylase biotin carboxyl carrier protein (AccB), and acetyl-CoA carboxylase (AccD) were marked increased by OH treatment, while decreased after repair; and ACP S-malonyltransferase (FabD) continued to increase slightly at both injured and end-repaired stages. In the fatty acid carbon chain extension pathway, the expression levels of enoyl-ACP reductase (FabI), beta-ketoacyl-ACP synthase II (FabF), and 3-hydroxyacyl-ACP dehydratase (FabZ) were increased due to sublethal injury and then declined after restoration. Fatty acid kinase catalytic subunit (FakA) and fatty acid kinase (FakB1, FakB2) are important enzymes in FASII bypass pathways. After the OH process, the expression level of FakA increased while FakB1 and FakB2 decreased. Upon entering the stable

restoration phase, FakA decreased slightly while FakB1 and FakB2 increased compared to unrepaired *S. aureus*. In terms of phosphatidic acid synthesis cellular phospholipid pathway, OH treatment notably increased the expression of CDP-diacylglycerol--glycerol-3-phosphate 3-phosphatidyltransferase (PgsA) and bifunctional lysylphosphatidylglycerol flippase/synthetase (MprF), while PgsA, MprF, and cardiolipin synthase (Cls) reduced at the end-repair stage. In addition, sublethal injury led to a remarkable decrease in aconitate hydratase (AcnA) expression in the SI group, and without recovery signs in the RE group.

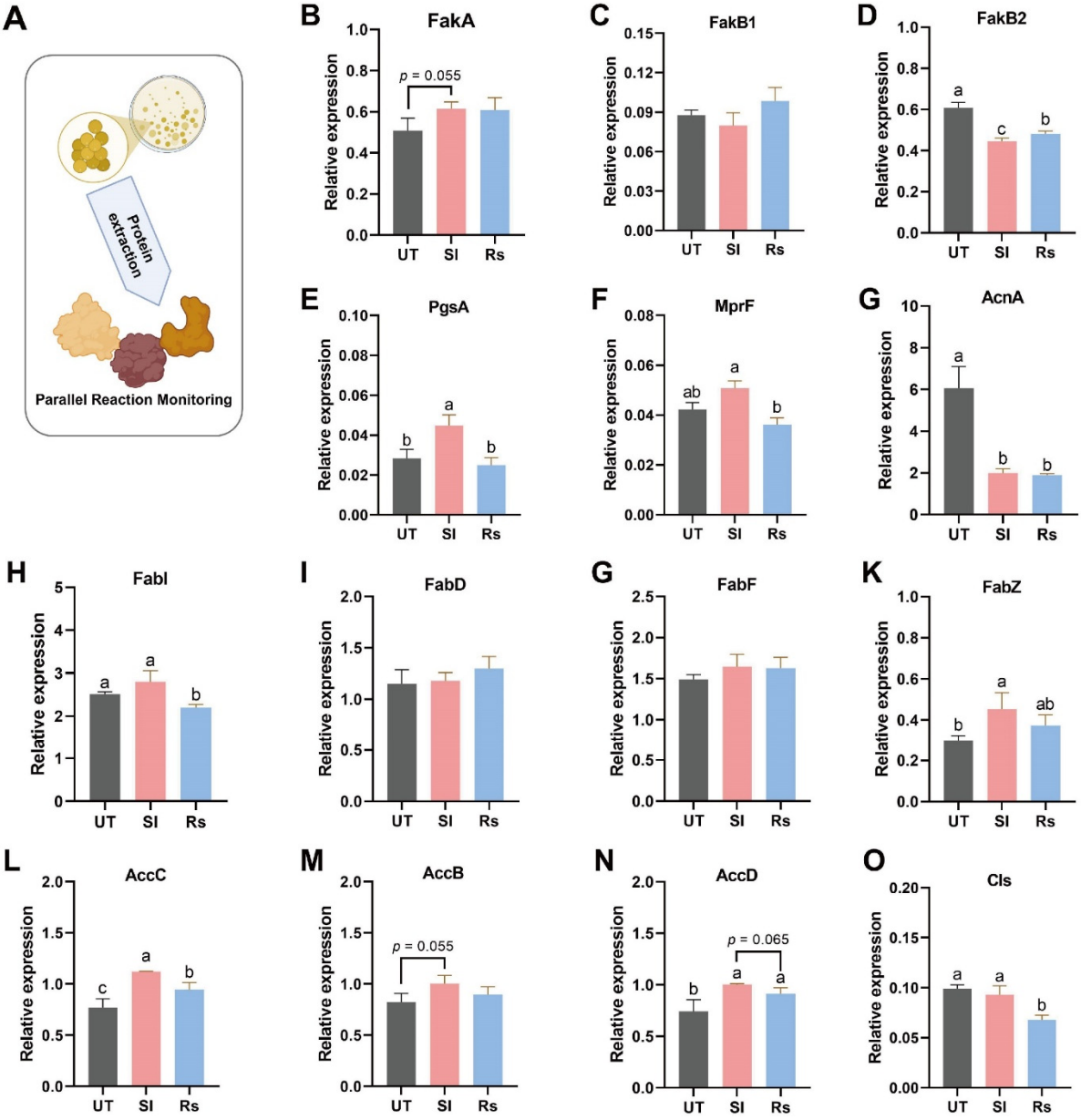

Figure 7. (A) *S. aureus* protein was extracted for parallel reaction monitoring analysis. (B)- (O) Expressions of cell membrane lipids synthesis-associated proteins in *S. aureus* after OH treatment and repair in NB. UT: untreated *S. aureus*; SI: OH-induced sublethally injured *S. aureus*; R_E: repaired *S. aureus*. Capital letters a ~ c represent the significant difference under different recovered time ($P < 0.05$).

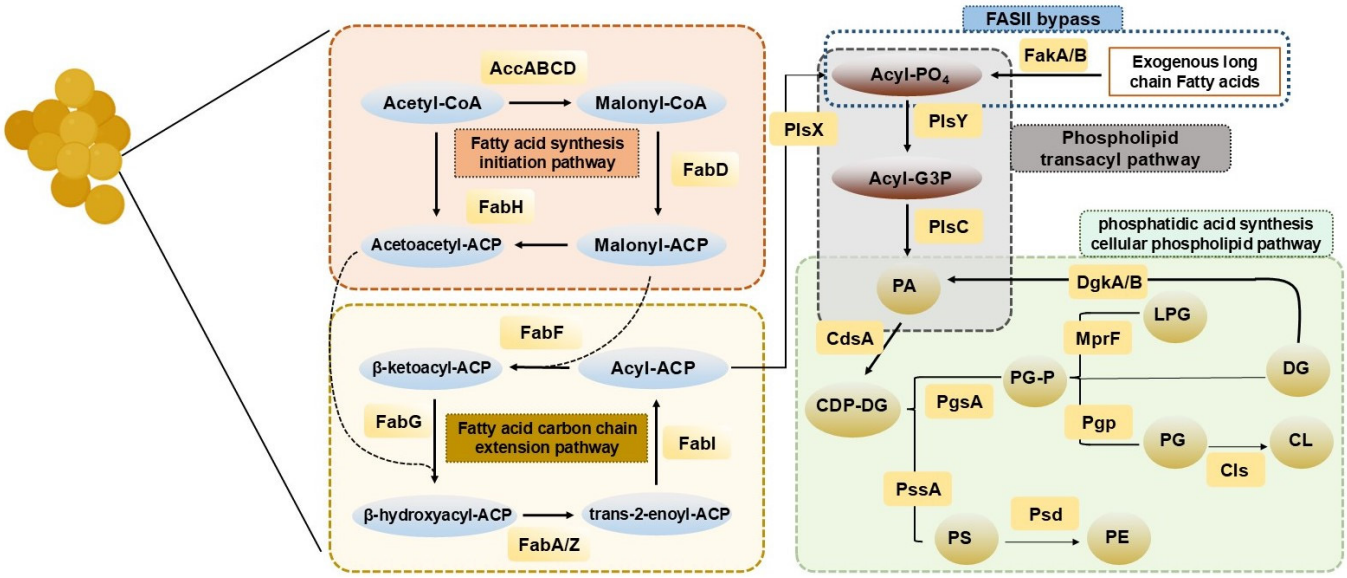

Figure 8. Lipid metabolism associated pathways in *S. aureus*.

Interestingly, key enzymes involved in lipid metabolism pathways, such as AccB, AccC, AccD, PgsA, MprF, FabI, FabZ, Cls, and FakA, exhibited changes consistent with lipid content trends. These enzymes were significantly upregulated after OH treatment and subsequently downregulated at the end-repair phase (Figure 6). The discrepancies between transcriptional and protein levels are likely due to extensive post-transcriptional and post-translational regulation. Gene expression involves both transcription (mRNA) and translation (protein), and several intermediate processes—such as mRNA degradation, translational efficiency, and post-translational modifications—can lead to temporal and spatial mismatches between mRNA and protein levels. For example, protein abundance may peak after mRNA degradation, or mRNA may rise while protein synthesis continues, Robles et al. [31] using *in vivo* SILAC labeling, demonstrated that protein levels oscillate in response to mRNA expression with a delay of up to six hours. Similarly, Zou, Zhang, Liang, Li, Chen, Wu [32] found that some gene showed trends opposite to those of their corresponding proteins. This is particularly relevant in stress responses, where mRNA levels often exhibit transient spikes, whereas protein expression is more sustained. Furthermore, environmental dynamic add complexity, as local availability of resources for translation can influence both transcript and protein abundances. As Liu pointed out, under steady-state conditions; however, during drastic environmental changes—such as OH-induced sublethal damage—post-transcriptional regulation may override this relationship [33].

While transcriptomic analysis alone may not fully capture bacterial metabolic activity, it provides valuable insights into gene-level responses. Ribosomes, which mediate translation, convert genetic information into proteins through amino acid polymerization [34]. In this study, differentially expressed genes (DEGs) from both the UT–SI and RE–SI comparisons were significantly enriched in the ribosomal pathway. Specifically, OH treatment resulted in the downregulation of 44 out of 45 ribosome-related DEGs, with only *rpsU* upregulated. In contrast, during the repair phase, 51 out of 54 ribosomal DEGs were upregulated, with only *rpsA*, *rpsU*, and *rpmB* remaining downregulated (Table S4). These results suggest that OH-induced stress impaired translational function, with selective gene expression retained to support essential survival

processes. This impairment appeared to be alleviated by the end of the repair phase, indicating a recovery of translational capacity. Supporting this, previous work from our laboratory demonstrated a gradual increase in protein content and restoration of protein bands during the repair process following OH treatment [10].

3.5 Applications in milk, parsley-kale juice, and tomato juice

The repair processes of OH-induced injured *S. aureus* in milk, parsley-kale juice and tomato juices are explored (Figure S4). It can be seen that due to the rich nutrition of milk, the number of bacteria increased markedly at both 4℃ and 25℃. At 4℃, the repair of injured *S. aureus* was partially inhibited. In addition, the milk emitted an unpleasant smell after being stored at 25℃ for 72 h. Although the pH of juices was low (4.00-4.45), the viable counts on NA and NA-NaCl plates suggest that injured *S. aureus* was able to survive for at least 72 h in juices at 4℃ and 25℃. Specifically, the number of *S. aureus* decreased parsley-kale juice during the first 0- 6 h at 4℃ and 25℃, then the number remained stable and the injured bacteria were difficult to complete repair when the storage temperature was 4℃. However, the injured bacteria are able to repair and continue to grow in number when the storage temperature was 25℃. For tomato juice, bacterial counts consistently decreased at both storage temperatures and were similarly difficult to repair at 4℃. In addition, samples stored at 25℃ had a darker color and a worse odor. These results highlight the importance of this study and indicate that low temperature is an effective method for inhibiting the repair of OH-induced injured *S. aureus*.

4. Conclusion

This study employed a multi-omics approach—integrating lipidomics, transcriptomics, and PRM—to elucidate the repair mechanisms of *Staphylococcus aureus* following sublethal injury induced by ohmic heating (OH). The results demonstrated that OH treatment significantly disrupted lipid metabolism, particularly affecting fatty acid metabolism and glycerophospholipid biosynthesis pathway. Key lipids, such as CL, PG, PE, and Cer, initially were upregulated in response to OH-induced stress, while their levels declined during the subsequent repair phase in NB. Changes in MDA content indicated that lipid oxidation damage caused by OH treatment was restored at the end-repair period. The observed decrease in malondialdehyde (MDA) levels further confirmed that oxidative lipid damage was alleviated upon repair. Interestingly, while lipid content and protein expression of metabolic enzymes followed similar trends, transcriptomic data revealed an inverse pattern, suggesting that extensive post-transcriptional and translational regulation occurs during bacterial recovery. This highlights the importance of integrating multi-omics data to capture the full complexity of cellular responses to sublethal stress. Finally, application experiments in milk, parsley–kale juice, and tomato juice indicated that low-temperature storage effectively suppresses the repair and proliferation of OH-injured *S. aureus*, underscoring practical strategies to mitigate food safety risks. Collectively, these findings advance our understanding of bacterial repair biology and support the broader application of OH in food processing. Future studies should further explore the regulatory networks governing lipid metabolism under stress and identify synergistic treatments to inhibit bacterial recovery in food matrices.

References

[1] S.R. Yousefi, H.A. Alshamsi, O. Amiri, et al., Synthesis, characterization and application of Co/Co3O4 nanocomposites as an effective photocatalyst for discoloration of organic dye contaminants in wastewater and antibacterial properties, Journal of Molecular Liquids. (2021) https://doi.org/10.1016/j.molliq.2021.116405.

[2] Z. Huang, X. Yu, Q. Yang, et al., Aptasensors for Staphylococcus aureus Risk Assessment in Food, Frontiers in Microbiology. (2021) https://doi.org/10.3389/fmicb.2021.714265.

[3] WHO, Food safety, (2024) https://doi.org/Retrieved from: https://www.who.int/health-topics/food-safety.

[4] W. Li, S.M. Pires, Z. Liu, et al., Surveillance of foodborne disease outbreaks in China, 2003–2017, Food Control. (2020) https://doi.org/10.1016/j.foodcont.2020.107359.

[5] M. Sakr, S. Liu, A comprehensive review on applications of ohmic heating (OH), Renewable and Sustainable Energy Reviews. 39 (2014) 262-269. https://doi.org/10.1016/j.rser.2014.07.061.

[6] H. Jaeger, A. Roth, S. Toepfl, et al., Opinion on the use of ohmic heating for the treatment of foods, Trends in Food Science & Technology. (2016) https://doi.org/10.1016/j.tifs.2016.07.007.

[7] X. Tian, Q. Yu, D. Yao, et al., New Insights Into the Response of Metabolome of Escherichia coli O157:H7 to Ohmic Heating Frontiers in Microbiology. 9 (2018) https://doi.org/10.3389/fmicb.2018.02936.

[8] L. Jia, L. Shao, Y. Zhao, et al., Inactivation effects and mechanism of ohmic heating on Bacillus cereus, International Journal of Food Microbiology. 390 (2023) 110125. https://doi.org/https://doi.org/10.1016/j.ijfoodmicro.2023.110125.

[9] L. Shao, Y. Liu, X. Tian, et al., Inactivation of Staphylococcus aureus in phosphate buffered saline and physiological saline using ohmic heating with different voltage gradient and frequency, Journal of Food Engineering. 274 (2020) 109834. https://doi.org/https://doi.org/10.1016/j.jfoodeng.2019.109834.

[10] W. Han, S. Lele, S. Yingying, et al., Recovery mechanisms of ohmic heating-induced sublethally injured Staphylococcus aureus: Changes in cellular structure and applications in pasteurized milk, Food Control. (2024) https://doi.org/10.1016/j.foodcont.2024.111086.

[11] L. Shao, Y. Zhao, B. Zou, et al., Recovery and virulence factors of sublethally injured Staphylococcus aureus after ohmic heating, Food Microbiology. 102 (2022) 103899. https://doi.org/https://doi.org/10.1016/j.fm.2021.103899.

[12] J.-Y. Hao, Y.-Q. Lei, J.-Y. Shi, et al., Integrative Physiological and Transcriptome Analysis Reveals the Mechanism for the Repair of Sub-Lethally Injured Escherichia coli O157: H7 Induced by High Hydrostatic Pressure, Foods. 11 (2022) 2377. https://doi.org/https://doi.org/10.3390/foods11152377.

[13] S.E. Hartsell, The longevity and behavior of pathogenic bacteria in frozen foods; the influence of plating media, American Journal of Public Health and the Nations Health. (1951) https://doi.org/10.2105/ajph.41.9.1072.

[14] M. Ferone, A. Gowen, S. Fanning, et al., Microbial detection and identification methods: Bench top assays to omics approaches, Comprehensive Reviews in Food Science and Food Safety. (2020) https://doi.org/10.1111/1541-4337.12618.

[15] R. Zhang, Z. Zhu, W. Jia, Molecular mechanism associated with the use of magnetic fermentation in modulating the dietary lipid composition and nutritional quality of goat milk, Food Chemistry. (2021) https://doi.org/10.1016/j.foodchem.2021.130554.

[16] R. Arias-Cartin, S. Grimaldi, P. Arnoux, et al., Cardiolipin binding in bacterial respiratory complexes: structural and functional implications, Biochimica et Biophysica Acta (BBA) - Bioenergetics. (2012) https://doi.org/10.1016/j.bbabio.2012.04.005.

[17] S.M. Claypool, Cardiolipin, a critical determinant of mitochondrial carrier protein assembly and function, Biochimica et Biophysica Acta (BBA) - Biomembranes. (2009) https://doi.org/10.1016/j.bbamem.2009.04.020.

[18] G. Korza, S. DePratti, D. Fairchild, et al., Expression of the 2Duf protein in wild-type Bacillus subtilis spores stabilizes inner membrane proteins and increases spore resistance to wet heat and hydrogen peroxide, Journal of Applied Microbiology. (2023) https://doi.org/10.1093/jambio/lxad040.

[19] K.K. Griffiths, P. Setlow, Effects of modification of membrane lipid composition on Bacillus subtilis sporulation and spore properties, Journal of Applied Microbiology. (2009) https://doi.org/10.1111/j.1365-2672.2009.04176.x.

[20] J. Walczak-Skierska, M. Złoch, K. Pauter, et al., Lipidomic analysis of lactic acid bacteria strains by matrix-assisted laser desorption/ionization time-of-flight mass spectrometry, Journal of Dairy Science. (2020) https://doi.org/10.3168/jds.2020-18753.

[21] W. Zhao, T. Róg, A.A. Gurtovenko, et al., Role of phosphatidylglycerols in the stability of bacterial membranes, Biochimie. (2008) https://doi.org/10.1016/j.biochi.2008.02.025.

[22] Y. Sun, Y. Liu, H. Wang, et al., Revealing the mechanism of ohmic heating against Bacillus cereus spores through intracellular homeostasis and lipid analysis, Food Control. (2024) https://doi.org/https://doi.org/10.1016/j.foodcont.2024.110972.

[23] O. Geiger, I.M. López-Lara, C. Sohlenkamp, Phosphatidylcholine biosynthesis and function in bacteria, Biochimica et Biophysica Acta (BBA) - Molecular and Cell Biology of Lipids. (2012) https://doi.org/10.1016/j.bbalip.2012.08.009.

[24] L. Amalia, S.-L. Tsai, Ceramide's Role and Biosynthesis: A Brief Review, Biotechnology and Bioprocess Engineering. (2023) https://doi.org/10.1007/s12257-022-0257-8.

[25] K. Hosomi, H. Kiyono, J. Kunisawa, Fatty acid metabolism in the host and commensal bacteria for the control of intestinal immune responses and diseases, Gut Microbes. (2019) https://doi.org/10.1080/19490976.2019.1612662.

[26] R. Jasim, M.-L. Han, Y. Zhu, et al., Lipidomic Analysis of the Outer Membrane Vesicles from Paired Polymyxin-Susceptible and -Resistant Klebsiella pneumoniae Clinical Isolates, International Journal of Molecular Sciences. (2018) https://doi.org/10.3390/ijms19082356.

[27] D. Pang, Z. Huang, Q. Li, et al., Antibacterial Mechanism of Cinnamaldehyde: Modulation of Biosynthesis of Phosphatidylethanolamine and Phosphatidylglycerol in Staphylococcus aureus and Escherichia coli, Journal of Agricultural and Food Chemistry. (2021) https://doi.org/10.1021/acs.jafc.1c04977.

[28] X. Tian, Q. Yu, L. Shao, et al., Comparative transcriptomic study of Escherichia coli O157:H7 in response to ohmic heating and conventional heating, Food Research International. 140 (2021) 109989. https://doi.org/https://doi.org/10.1016/j.foodres.2020.109989.

[29] L. Shao, Y. Liu, Y. Zhao, et al., Integrated transcriptomic and metabolomic analysis of the global response of Staphylococcus aureus to ohmic heating, Innovative Food Science & Emerging Technologies. 74 (2021) 102870. https://doi.org/https://doi.org/10.1016/j.ifset.2021.102870.

[30] J. Yao, C.O. Rock, Bacterial fatty acid metabolism in modern antibiotic discovery, Biochimica et Biophysica Acta (BBA) - Molecular and Cell Biology of Lipids. (2016) https://doi.org/10.1016/j.bbalip.2016.09.014.

[31] M.S. Robles, J. Cox, M. Mann, In-vivo quantitative proteomics reveals a key contribution of post-transcriptional mechanisms to the circadian regulation of liver metabolism, PLOS Genetics. (2014) https://doi.org/10.1371/journal.pgen.1004047.

[32] H. Zou, B. Zhang, H. Liang, et al., Defence mechanisms of Pinctada fucata martensii to Vibrio parahaemolyticus infection: Insights from proteomics and metabolomics, Fish & Shellfish Immunology. (2023) https://doi.org/10.1016/j.fsi.2023.109204.

[33] Y. Liu, A. Beyer, R. Aebersold, On the Dependency of Cellular Protein Levels on mRNA Abundance, Cell. (2016) https://doi.org/10.1016/j.cell.2016.03.014.

[34] T. Wang, C. Liang, M. Zheng, et al., Ribosome Hibernation as a Stress Response of Bacteria, Protein & Peptide Letters. (2020) https://doi.org/10.2174/0929866527666200610142118.